Modeling of Ground-Penetrating Radar for Detecting Buried Objects in Dispersive Soils

K. P. Prokopidis and T. D. Tsiboukis

Applied and Computational Electromagnetics Laboratory,
Department of Electrical and Computer Engineering,
Aristotle University of Thessaloniki, Thessaloniki, GR 54124, Greece
E-mail: kprokopi@faraday.ee.auth.gr; tsibukis@auth.gr

Abstract − The detection of buried targets with ground-penetrating radars (GPRs) has been an issue of considerable attention during the last decades. In this paper, an efficient three-dimensional (3-D) time-domain numerical method is proposed for the simulation of GPR on dispersive soils. The soil is considered as an M-th order Debye medium with additional static conductivity and an unsplit-field perfectly matched layer (PML) is also presented to terminate such media. The radar unit is modeled with two transmitters and one receiver in order to eliminate undesired signals. The impact of radar frequency, soil parameters and object depth upon the ability to detect buried targets is investigated through several finite-difference time-domain (FDTD) simulations. The detection of multiple dielectric and conducting buried objects in stratified and inhomogeneous soils can be feasible through the tracing of the received energy of B-scan measurements in perpendicular linear paths.

Index Terms − Finite difference time domain (FDTD) method, ground-penetrating radar, dispersive media, perfectly matched layer.

I. INTRODUCTION

There is a growing interest in the propagation of transient electromagnetic signals through the earth and subsurface radar techniques for the detection and location of buried artifacts and structures within the upper regions of the earth's surface [1]-[6]. Ground-penetrating radar (GPR) has a wide range of applications such as geological mapping, object detection, and various archeological, civil and electrical engineering applications. The algorithm uses transmitting and receiving antennas placed near the earth's surface to probe the shallow subsurface. It is well known that at the GPR operating range (50-1000

MHz) soil is dispersive. More specifically, the dielectric constant and conductivity of the earth are functions of the excitation frequency.

The finite-difference time-domain (FDTD) method [7], [8] is inarguably one of the most successful second-order accurate schemes for electromagnetic time-domain simulations. Although the applicability of the original FDTD scheme is restricted to nondispersive media, a number of researchers have extended the conventional Yee's scheme to incorporate dispersive media. There are several techniques, like the recursive convolution (RC) [7], the auxiliary differential equation (ADE) scheme [8], the Z-transform (ZT) [9] and some alternative techniques [10]-[12] for handling dispersive media. An extensive survey of the FDTD methods for dispersive media is found in [13] and in the introduction of [4]. Among the previous techniques, we select a competent modification of the ADE approach [10] and introduce an unsplit-field perfectly matched layer (PML) which is used to terminate the computational domain.

Since the FDTD technique is very easy to implement, versatile and can handle any number and type of scatterers and soils, it has been extensively used to simulate GPR problems [2]-[6]. Usually, in the FDTD simulations, the soil is modeled as a dielectric with constant permittivity. In contrast, this paper presents a complete FDTD simulation with a practical radar configuration and introduces a number of simple techniques for the detection of dielectric and/or conducting buried targets in various realistic ground models.

II. FDTD/PML METHOD FOR THE DEBYE MODEL

Although the determination of the dielectric properties of earth materials remains largely experimental there is always the need of soil modeling. Experimental data indicate that dielectric behavior of wet snow, rocks, soils

and even dry sand follows the Debye relaxation [1], [14]. This good fit to the Debye model with multiple poles is explained by the natural occurring of moisture in varying proportions everywhere in earth. The relative complex dielectric permittivity $\varepsilon_r(\omega)$ for the case of the M-th order Debye medium ($e^{j\omega t}$ time variation is assumed) is described by the following equation

$$\varepsilon_r(\omega) = \varepsilon_{r,\infty} + \sum_{p=1}^{M} \frac{\varepsilon_{r,sp} - \varepsilon_{r,\infty}}{1 + j\omega\tau_p} \tag{1}$$

where $\varepsilon_{r,sp}$, τ_p is the relative static permittivity and the relaxation time of the p pole, respectively, and $\varepsilon_{r,\infty}$ is the infinite relative permittivity usually determined to fit experimental data.

For the FDTD simulations we adopt the efficient technique of [10] and we propose a new PML formulation to terminate the simulation region. The modified Maxwell's equations inside the PML are written as,

$$\nabla \times \tilde{\mathbf{H}} = j\omega\varepsilon_0 \left[\frac{\sigma}{j\omega\varepsilon_0} + \varepsilon_r(\omega) \right] T \cdot \tilde{\mathbf{E}}, \tag{2}$$

$$\nabla \times \tilde{\mathbf{E}} = -j\omega\mu_0 T \cdot \tilde{\mathbf{H}}, \tag{3}$$

where the terminated medium is assumed to be dispersive with relative permittivity $\varepsilon_r(\omega)$ and additional static conductivity σ and $T = \text{diag}\{\zeta_x/(\zeta_y\zeta_z)$, $\zeta_y/(\zeta_z\zeta_x)$, $\zeta_z/(\zeta_x\zeta_y)\}$ is the diagonal "material" tensor of the PML conductivities. The tilde denotes that the fields are in the frequency domain. The stretching factors ζ_s are defined as $\zeta_s = 1/[\kappa_s + \sigma_s/(j\omega)]$, $s = x, y, z$ where κ_s and σ_s are spatially polynomial variables.

Ampere's law, equation (2), is written as

$$\nabla \times \tilde{\mathbf{H}} = \sigma T \cdot \tilde{\mathbf{E}} + j\omega\varepsilon_\infty T \cdot \tilde{\mathbf{E}} + j\omega \sum_{p=1}^{M} \tilde{\mathbf{Q}}_p \tag{4}$$

where $\varepsilon_\infty = \varepsilon_0\varepsilon_{r,\infty}$. The additional variable $\tilde{\mathbf{Q}}_p$ is defined as,

$$\tilde{\mathbf{Q}}_p = \frac{\varepsilon_{sp} - \varepsilon_\infty}{1 + j\omega\tau_p} T \cdot \tilde{\mathbf{E}} \tag{5}$$

with $\varepsilon_{sp} = \varepsilon_0\varepsilon_{r,sp}$. We also introduce variables $\tilde{\mathbf{R}} = T \cdot \tilde{\mathbf{E}}$ and equation (4) takes the following form

$$\nabla \times \tilde{\mathbf{H}} = \sigma\tilde{\mathbf{R}} + j\omega\varepsilon_\infty\tilde{\mathbf{R}} + j\omega \sum_{p=1}^{M} \tilde{\mathbf{Q}}_p . \tag{6}$$

We next transform equations (5) and (6) into the time domain and get

$$\mathbf{Q}_p + \tau_p \frac{d\mathbf{Q}_p}{dt} = (\varepsilon_{sp} - \varepsilon_\infty)\mathbf{R}, \tag{7}$$

$$\nabla \times \mathbf{H} = \sigma\mathbf{R} + \varepsilon_\infty \frac{d\mathbf{R}}{dt} + \sum_{p=1}^{M} \frac{d\mathbf{Q}_p}{dt} . \tag{8}$$

Equations (7) and (8) are approximated using finite differences and the update equations for the variables $\mathbf{Q}_p$ and $\mathbf{R}$ are

$$\mathbf{Q}_p^{n+1} = \frac{2\tau_p - \Delta t}{2\tau_p + \Delta t}\mathbf{Q}_p^n + \frac{(\varepsilon_{sp} - \varepsilon_\infty)\Delta t}{2\tau_p + \Delta t}\left(\mathbf{R}^{n+1} + \mathbf{R}^n\right), \tag{9}$$

$$\mathbf{R}^{n+1} = c_e\mathbf{R}^n + c_m(\nabla \times \mathbf{H})^{n+1/2} + 2c_m\sum_{p=1}^{M} \frac{1}{2\tau_p + \Delta t}\mathbf{Q}_p^n , \tag{10}$$

where Δt is the time step of the FDTD method and the coefficients c_e and c_m are given by

$$c_e = \frac{2\varepsilon_\infty - \sigma\Delta t - 2\sum_{p=1}^{M} \frac{(\varepsilon_{sp} - \varepsilon_\infty)\Delta t}{2\tau_p + \Delta t}}{2\varepsilon_\infty + \sigma\Delta t + 2\sum_{p=1}^{M} \frac{(\varepsilon_{sp} - \varepsilon_\infty)\Delta t}{2\tau_p + \Delta t}},$$

$$c_m = \frac{2\Delta t}{2\varepsilon_\infty + \sigma\Delta t + 2\sum_{p=1}^{M} \frac{(\varepsilon_{sp} - \varepsilon_\infty)\Delta t}{2\tau_p + \Delta t}}. \tag{11}$$

The x-component of the variable $\mathbf{R}$ is $\tilde{R}_x = \zeta_x/(\zeta_y\zeta_z)\tilde{E}_x$ and the update equation for E_x is obtained following the methodology of [15]. The FDTD/PML equations for the other electric and magnetic components can be extracted in the same fashion.

Since all explicit finite-difference schemes are conditionally stable, there is the need for the stability condition of the proposed formulation. The fields are expressed as [16]

$$\mathbf{F}^n = \mathbf{F}_0 Z^n e^{j(I\Delta x\tilde{k}_x + J\Delta y\tilde{k}_y + K\Delta z\tilde{k}_z)} \tag{12}$$

where $\mathbf{F}_0$ is a complex amplitude, indexes I, J, K denote the positions of the nodes in the FDTD grid, $\Delta\beta, (\beta = x, y, z)$ are the sizes of the FDTD cells, $\tilde{k}_\beta, (\beta = x, y, z)$ is the numerical wavenumber in the β-direction and Z is a complex variable. Such solutions are substituted into the difference equations and the characteristic polynomial is yielded (for the case of the one-pole Debye medium is a third-order polynomial). The condition for stability can be written as $|Z_i| \leq 1$, where Z_i are the roots of the characteristic polynomial in Z. Since the characteristic polynomial is generally dependent on the Debye parameters, the maximum value of the time step Δt cannot be independently specified as it is with nondispersive media. Given the parameters of the medium and $\Delta\beta$, the selection of Δt is tested by numerically finding the roots of the characteristic polynomial. For the case of the one-pole Debye medium, the stability criterion of the proposed scheme can be expressed as

$$\Delta t \le \frac{1}{c_\infty} \left(\sum_{\beta=x,y,z} \frac{1}{(\Delta\beta)^2} \right)^{-1/2} \tag{13}$$

where $c_\infty = 1/\sqrt{\mu\varepsilon_\infty}$ on condition that $\varepsilon_s \ge \varepsilon_\infty$.

III. SOIL PARAMETERS AND RADAR UNIT

In this paper, the radar unit consists of two identical transmitters (T_1 and T_2) and one receiver (R), called transmitter-receiver-transmitter (TRT) configuration [5], illustrated in Fig. 1. The two alike transmitters, modeled as small electric dipoles aligned at z-axis, are fed $180°$ out of phase and the receiver is located equidistantly between them. The receiver is implemented as a small dipole which samples and stores the z-component of the electric field at a specific Yee cell. Due to this configuration, the two direct signals D_1 and D_2 are mutually cancelled at the receiver R. Similarly, the two reflected signals G_1 and G_2 are subtracted at the same symmetry plane and they do not contribute to the signal received by the receiver. Finally, the signal collected by the receiver is solely due to the scatterers buried in the ground. Using this configuration, we separate the desired scattered signal $S_1 + S_2$, which is generally weak, from the direct and the reflected from the ground signal, rendering thus, the buried-object detection procedure possible.

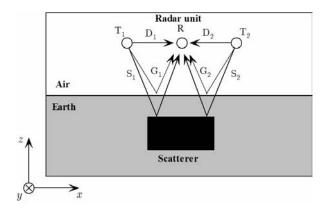An A-scan is performed when the radar unit is

Fig. 1. The TRT configuration of the radar unit with the direct (D_1 and D_2), the reflected (G_1 and G_2), and the scattered (S_1 and S_2) signals depicted.

stationary and the receiver collects data for a time period. When the radar unit travels along a linear path performing repeated A-scan measurements at discrete points above the ground, this is called B-scan [5]. For our simulations the radar unit moves in a linear path performing B-scan

simulations. The fields are excited using hard sources at the points of the two transmitters. The time variation of the source is given by $f(n) = e^{-a[(n-b)\Delta t]^2} \cos(2\pi f_c n \Delta t)$, where $b = 512$, $a = 16/(\beta \Delta t)^2$, f_c the excitation frequency and n denotes the time step.

IV. NUMERICAL RESULTS

In our FDTD simulations, the Yee cell sizes are selected to be $\Delta = \Delta x = \Delta y = \Delta z = 5\,\text{cm}$ and the time step $\Delta t = 38.516\,\text{psec}$, in order to ensure the stability. The size of the computational domain is $60 \times 60 \times 30$ Yee cells and is truncated with an 8-cell PML described in previous section. The transmitting and receiving antennas are arranged as shown in Fig. 1 and are separated by two cells (10 cm). The radar unit is moving in straight lines and is located 10 cm above the ground surface. We assume three Puerto Rico clay loams modeled with Debye dispersion with parameters listed in Table I [4]. The soil occupies the first 20 cells of the vertical height of the simulation region.

Table I. Model parameters for Puerto Rico clay loams.

Moisture (%)	$\varepsilon_{r,\infty}$	σ (mS/m)	τ_1 (nsec)	τ_2 (nsec)	$\varepsilon_{r,s1}$	$\varepsilon_{r,s2}$
2.5	3.20	0.397	2.71	0.108	3.95	3.50
5.0	4.15	1.110	3.79	0.151	5.95	4.75
10.0	6.00	2.000	3.98	0.251	8.75	6.75

We assume two cubic scatterers: a perfectly electric conductor (PEC) and a dielectric one with permittivity $8\varepsilon_0$. The PEC and the dielectric targets of sizes $5\Delta \times 5\Delta \times 5\Delta$ and $4\Delta \times 4\Delta \times 4\Delta$ are buried 4Δ and 5Δ under the ground-air interface, respectively and are separated by 6Δ. In Fig. 2 the electric field at the receiver is depicted when one scatterer, both scatterers and no scatterers are present. The scatterers are buried in 2.5 % moisture soil with parameters taken from Table I. It is obvious, as expected, that the received signal is solely due to buried objects.

In the following, we show two FDTD snapshots of the x-component of the electric field for the TRT radar model above earth modeled with two different Debye media for the aforementioned scenario of the two scatterers. The central frequency of excitation is 200 MHz. In Fig. 3 (a) the earth is modeled with the Debye model of 2.5 % moisture while in Fig. 3 (b) with the 5 % moisture. We can observe the wave propagation in free space and dispersive soil and the scattering from the two targets.

Since the detection of buried targets is performed

Fig. 2. The electric field at the receiver of a TRT radar as a function of time for different subsurface scenarios (A-scan).
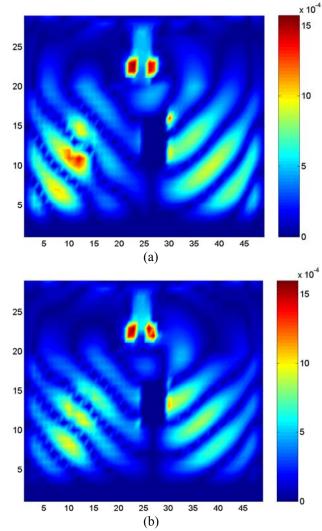

(a)

(b)

Fig. 3. Snapshots of the amplitude of the x-component of the electric field. The ground is modeled with Debye medium of (a) 2.5 % and (b) 5 % moisture.

through the received energy due to the presence of the scatterers, we estimate the scattered energy collected by the receiver in an A-scan, as $\mathcal{E} = \sum_n |E^n|^2$, where E^n is the n-th time sample of the corresponding electric field at that A-scan location.

A. Effect of Frequency

In order to investigate the effect of excitation frequency upon the operation of the GPR, we assume the aforementioned scenario with the Puerto Rico clay loam of 2.5 % moisture. We perform two simulations: (a) with $f_c = 200 \, \text{MHz}$ and (b) with $f_c = 400 \, \text{MHz}$ whereas the corresponding energy of the excitation functions is calculated as $\mathcal{E}_{t1} = 80.212$ and $\mathcal{E}_{t2} = 80.212$ (the energies are almost equal due to the value of the parameter b). Each A-scan is normalized with its own maximum and individually plotted in Figs 4 (a) and 4 (b) and form the B-scan plot which is a function of the position of the radar unit (vertical axis) and time (horizontal axis). In Figs 4 (a) and 4 (b), the energies of the A-scans waveforms are depicted as a function of the radar position (vertical axis). The maximum energy collected by the receiver is $\mathcal{E}_{r1} = 85.281$ and $\mathcal{E}_{r2} = 102.123$. The ratios of the received to the transmitted energy for the two frequencies are 1.063 and 1.273, respectively. So, the PEC target is better detected if excitation frequency is $f_c = 400 \, \text{MHz}$, although the position of the dielectric target is not very clear for this case. We also remark that the energy peak for the conducting target is greater than that of the dielectric as expected.

B. Effect of Soil Parameters and Object Depth

Usually, there is great difficulty in accurate prediction of the electromagnetic propagation behavior of the ground due to the variability of the material parameters and local geological conditions encountered in real life. We now perform another set of numerical simulations in which the parameters of the ground are that of the Puerto Rico clay loam with 5 % moisture (Table I) which describes a wet earth, to investigate the effect of soil parameters. Fig. 5 (a) shows the same scenario as in the previous subsection but in another soil background (with 5 % moisture) for $f_c = 400 \, \text{MHz}$. The ratio of the collected to the transmitted energy is now 1.045. In Fig. 5 (b), the excitation frequency is 200 MHz, while the ratio is 0.996. We observe that using a higher frequency (400 MHz) we get 1.05 times more energy (Figs 5 (a) and 5 (b)) for the 5 % moisture model, whereas for the 2.5 % moisture model we obtain 1.2 (Figs 4 (a) and 4 (b)). This is due to the fact that the 5 % moisture soil model
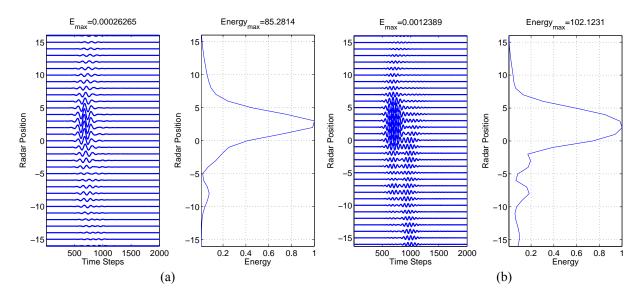
Fig. 4. Simulations results (B-scan and collected energy) of two scatterers (one PEC and one dielectric) buried 20 cm and 25 cm, respectively, under the ground and separated by 30 cm with excitation frequency (a) $f_c = 200\,\text{MHz}$, (b) $f_c = 400\,\text{MHz}$. The earth is a Puerto Rico clay loam with 2.5 % moisture.

containing more moisture than the 2.5 % causes greater attenuation to the scattered energy collected by the receiver. At a given frequency, wet materials exhibit higher dielectric losses than dry ones.

We next consider that the dielectric scatterer is smaller (of size $2\Delta \times 2\Delta \times 2\Delta$) and is buried 7Δ under the surface. The corresponding B-scan results are depicted in Fig. 5 (c). One may note that the dielectric scatterer is, now, invisible to the radar, since the collected energy is practically zero. Obviously, the scattered energy from the dielectric target is very weak due to the attenuation of the wet soil. It is to be stressed that in many practical applications, the GPR results are inconclusive because of the significant attenuation caused by the dispersive soil. Such problems can usually be solved with a proper frequency selection. Additionally, it is not plain to predict, before the FDTD simulation, which frequency is suitable, leads to less dielectric losses and to clear subsurface image.

C. Multiple Target Detection in Stratified Soil

One of the important goals of the GPR applications is to image metallic, dielectric scatterers and cavities in the near subsurface. We now assume a scenario with two perfectly conducting scatterers of sizes $3\Delta \times 3\Delta \times 3\Delta$ buried 4Δ under the ground. The earth model is assumed to be inhomogeneous and consists of a 25 cm thick layer of Puerto Rico clay loam with 5 % moisture near the surface and the rest of a 10 % moisture soil (with

parameters listed in Table I). The locations of the targets are illustrated in Fig. 6. Two linear, perpendicular paths (linear paths A and B in Fig. 6) are regarded. We perform B-scans upon the prementioned linear paths and the results are demonstrated in Figs 7 (a) and 7 (b). The maxima in the plots correspond to the energy scattered by the two targets, while the energy magnitudes are generally functions of the sizes, locations, depths and constitutive properties of the scatterers. Since in the examined scenario, the targets are the same in size and dielectric properties and are buried in the same depth, the energy peaks just indicate their locations. The prescribed procedure serves as a simple algorithm for the detection of buried targets and if combined with other measurements or calculations can provide an accurate subsurface image.

D. Target Detection in Inhomogeneous Soil

We now assume a more realistic scenario of earth model considering 50 small dielectric scatterers with permittivity $8\varepsilon_0$ of sizes and positions selected randomly embedded in a 2.5 % moisture soil background. The maximum size of the dielectric scatterers is $5\Delta \times 5\Delta \times 5\Delta$ and the excitation frequency is 200 MHz. A PEC target of size $5\Delta \times 5\Delta \times 5\Delta$ is buried 4Δ deep as shown in Fig. 8 (a). The maximum of the collected energy in Fig 8 (b) is due to PEC scatterer (this can be extracted by comparisons with previous B-scan simulations where the PEC scatterer was in the same position) although the

(a)   (b)   (c)
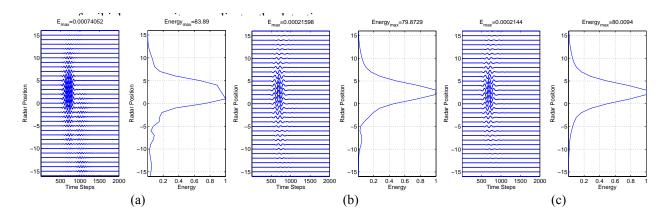
Fig. 5. Simulations results (B-scan and collected energy) of two scatterers (one PEC and one dielectric) (a), (b) buried 20 cm and 25 cm, respectively, under the ground and separated by 30 cm and (c) buried 20 cm and 35 cm, respectively, under the ground and separated by 40 cm with excitation frequency (a) $f_c = 400\,\text{MHz}$ and (b), (c) $f_c = 200\,\text{MHz}$. The earth is a Puerto Rico clay loam with 5.0 % moisture.
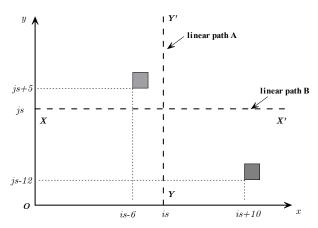

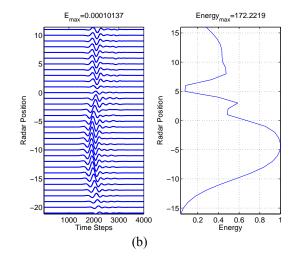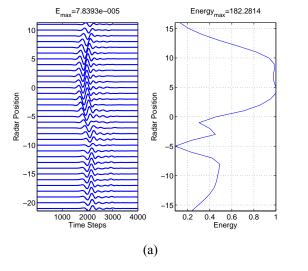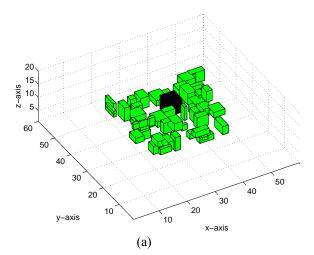Fig. 6.   Subsurface model with two perfectly electric conducting scatterers.

(b)

Fig. 7. Simulations results (B-scan and collected energy) of two perfectly electric conducting scatterers buried 4 cells under the ground: (a) linear path A and (b) linear path B.
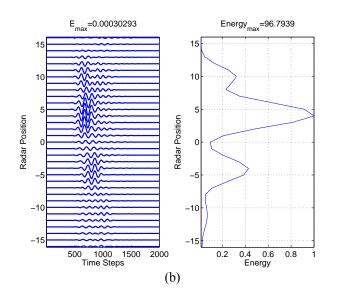

(a)

(a)

Fig. 8. (a) Inhomogeneous earth model (the PEC target and the dielectric scatterers are depicted) and (b) simulation results (B-scan and collected energy) for the inhomogeneous earth model with excitation frequency $f_c = 200\,\text{MHz}$.

V. CONCLUSIONS

The application and importance of the realistic ground model in the 3-D FDTD simulations of GPR scenarios are presented. The earth is modeled as a Debye medium with two poles and static conductivity and an efficient FDTD scheme is used to simulate the wave propagation inside stratified and inhomogeneous dispersive soils. An unsplit-field PML is also proposed for the termination of the computational domain and its effectiveness and accuracy is proved in numerous GPR problems with different (PEC or dielectric) targets and soil parameters. The effect of the excitation frequency upon the ability to detect buried objects is studied and the difficulty to recognize dielectric targets is discussed. The simulation results show that the detection of metal and dielectric buried objects is possible through the collected energy at the receiver and a simple and efficient algorithm is also introduced for the detection of multiple targets. The FDTD/PML technique presented in this paper provides a vigorous and effortless method for accurate GPR simulations and facilitate the analysis and design of GPR systems.

REFERENCES

[1] D. J. Daniels, *Surface-Penetrating Radar*, London, UK: IEE, 1996.

[2] J. M. Bourgeois and G. S. Smith, "A fully three-dimensional simulation of a ground-penetrating radar: FDTD theory compared with experiment," *IEEE Trans. Geosci. Remote Sensing*, vol. 34, pp. 36-44, Jan. 1996.

[3] T. Bergmann, J. O. A. Robertsson, and K. Holliger, "Finite-difference modeling of electromagnetic wave propagation in dispersive and attenuating media," *Geophysics*, vol. 63, pp. 856-867, May-June 1998.

[4] F. L. Teixeira, W. C. Chew, M. Straka, M. L. Oristaglio, and T. Wang, "Finite-difference time-domain simulation of ground penetrating radar on dispersive, inhomogeneous, and conductive soils," *IEEE Trans. Geosci. Remote Sensing*, vol. 36, pp. 1928-1937, Nov. 1998.

[5] L. Gurel and U. Oguz, "Three-dimensional FDTD modeling of a ground-penetrating radar," *IEEE Trans. Geosci. Remote Sensing*, vol. 38, pp. 1513-1521, July 2000.

[6] D. Uduwawala, M. Norgren, and P. Fuks, "A complete FDTD simulation of a real GPR antenna system operating above lossy and dispersive grounds," *Progress in Electromagnetics Research*, vol. 50, pp. 209-229, 2005.

[7] K. Kunz and R. Luebbers, *The Finite Difference Time Domain Method for Electromagnetics*, Boca Raton, FL: CRC, 1993

[8] A. Taflove and S. C. Hagness, *Computational Electrodynamics: The Finite-Difference Time-Domain Method*, Norwood, MA: Artech House, 2000.

[9] D. M. Sullivan, "Frequency-dependent FDTD methods using Z transforms," *IEEE Trans. Antennas Propagat.*, vol. 40, pp. 1223-1230, Oct. 1992.

[10] Y. Takayama and W. Klaus, "Reinterpretation of the Auxiliary Differential Equation method for FDTD," *IEEE Microw. Wireless Components Lett.*, vol. 12, pp. 102-104, Mar. 2002.

[11] J. A. Pereda, A. Vegas, and A. Prieto, "FDTD modeling of wave propagation in dispersive media by using the Mobius transformation technique," *IEEE Trans. Microw. Theory Tech.*, vol. 50, pp. 1689-1695, July 2002.

[12] K. P. Prokopidis, E. P. Kosmidou, and T. D. Tsiboukis, "An FDTD algorithm for wave propagation in dispersive media using higher-order schemes," *J. Electromagn. Waves Applicat.*, vol. 18, pp. 1171-1194, 2004.

[13] J. L. Young and R. O. Nelson, "A summary and systematic analysis of FDTD algorithms for linearly dispersive media," *IEEE Antennas Propagat. Mag.*, vol. 43, pp. 61-77, Feb. 2001.

[14] C. Matzler, "Microwave permittivity of dry sand," *IEEE Trans. Geosci. Remote Sensing*, vol. 36, pp. 317-319, Jan. 1998.

[15] S. D. Gedney, "An anisotropic perfectly matched layer-absorbing medium for the truncation of FDTD lattices," *IEEE Trans. Antennas Propagat.*, vol. 44, pp. 1630-1639, Dec. 1996.

[16] J. A. Pereda, L. A. Vielva, A. Vegas, and A. Prieto, "Analyzing the stability of the FDTD technique by combining the von Neumann method with Routh-Hurwitz criterion," *IEEE Trans. Microw. Theory Tech.*, vol. 49, pp. 377-381, Feb. 2001.

Konstantinos P. Prokopidis was born in Florina, Greece, on August 10, 1976. He received his Diploma Degree from the Department of Electrical and Computer Engineering (DECE), Aristotle University of Thessaloniki (A.U.Th.), Thessaloniki, Greece in 1999. From 2000 to 2001 he served as sergeant in the Hellenic Army (infantry). In 2001 he joined the Applied and Computational Electromagnetics Laboratory of the DECE, A.U.Th, where he is now pursuing his Ph. D. Degree. His research interests focus on finite difference time domain method, perfectly matched layers, higher-order schemes, dispersive media, antenna design, and signal processing. He is the recipient of a number of scholarship distinctions, including Technical Chamber of Greece Award and IRAKLITOS-Fellowship of research of the A.U.Th. Mr. Prokopidis is a member of the Technical Chamber of Greece and the Applied Computational Electromagnetics Society.

Theodoros D. Tsiboukis received the Diploma Degree in Electrical and Mechanical Engineering from the National Technical University of Athens, Greece, in 1971 and the Doctor Engineer Degree from the Aristotle University of Thessaloniki (A.U.Th.), Greece, in 1981. From 1981 to 1982, he joined the Electrical Engineering Department of the University of Southampton, England, as a senior research fellow. Since 1982 he has been working at the Department of Electrical and Computer Engineering (DECE) of the A.U.Th., where he is now a Professor. His main research interests include electromagnetic field analysis by energy methods, computational electromagnetics (FEM, BEM, Vector Finite Elements, MoM, FDTD, ABCs), inverse and EMC problems. He has authored or co-authored 6 books, more than 115 refereed journal articles, and more than 100 international conference papers. Prof. Tsiboukis was the Guest Editor of a special issue of the International Journal of Theoretical Electrotechnics (1996) and the Chairman of the local organizing committee of the 8th International Symposium on Theoretical Electrical Engineering (1995). He has served in many administrative positions, including Director of the Division of Telecommunications at the DECE (1993-1998) and Chairman of the DECE (1997-1998). Prof. Tsiboukis was awarded several distinctions and is member of various societies, associations, chambers and institutions.